The Metallicity Distribution in the Outer Halo of M33

R. Scott Brooks, Christine D. Wilson, and William E. Harris

Department of Physics and Astronomy, McMaster University, Hamilton, ON L8S 4M1, Canada

ABSTRACT

We present the results of deep I and V-band photometry of the halo stars near the southeast minor axis of the Local Group spiral galaxy M33. An $(I, V-I)$ color-magnitude diagram distinctly reveals the red giant branch stars at the bright end of the color-magnitude diagram. A luminosity function in the I-band which utilizes a background field to remove the contaminating effects of Galactic foreground stars and distant, unresolved galaxies reveals the presence of the tip of the red giant branch at $(m-M)_I = 20.70 \pm 0.10$. Assuming an absolute magnitude of the tip of the red giant branch of $M_{I,TRGB} = -4.1 \pm 0.1$ and a foreground reddening of $E(V-I) = 0.054 \pm 0.020$, the distance modulus of M33 is determined to be $(m-M)_\circ = 24.72 \pm 0.14$ (880 ± 60 kpc). The metallicity distribution function derived by interpolating between evolutionary tracks of red giant branch models is dominated by a relatively metal poor stellar population, with a mean metallicity of $[m/\mathrm{H}] = -0.94 \pm 0.04$ or $[\mathrm{Fe/H}] = -1.24$. We fit a leaky-box chemical enrichment model to the halo data, which shows that the halo is well represented by a single-component model with an effective yield of $y_{eff} = 0.0024$. The mean metallicity of a sample of globular clusters in the M33 halo ($[\mathrm{Fe/H}] = -1.3 \pm 0.1$) matches very closely the metallicity of the halo, but the cluster sample is too small to investigate other aspects of the metallicity distribution function of the clusters.

Subject headings: galaxies: halos—galaxies: individual (M31)—galaxies: photometry—galaxies: stellar content—Local Group

1. Introduction

Our current understanding of galaxy formation and evolution has improved in recent years; however, direct observation of these processes still lies beyond the ability of the current generation of telescopes. To better understand these issues, we must rely on secondary

properties that trace galactic formation and evolution. For the majority of galaxies, globular cluster systems and stellar halos serve as excellent diagnostic tracers of a galaxy's chemical evolution. Unfortunately, the majority of galaxies lie at distances too great to resolve individual stars and so studies of galactic stellar halos are limited to only the closest galaxies.

The halo of the Milky Way has yielded a wealth of information regarding the early stages of its chemical evolution. The bi-modal metallicity distribution of the Milky Way globular cluster system has been well established, a characteristic shared with many large spirals and giant ellipticals (Harris 2001). However, being embedded in the Galactic disk makes studies of individual halo stars difficult due to significant contamination from disk stars and the requirement of accurate relative distances to each halo object observed. Extragalactic globular cluster systems and stellar halos provide an opportunity to study stellar populations at roughly the same relative distance, thus eliminating the need for accurate distances to each halo object. Individual halo stars are easily resolved in M31, the largest galaxy in the Local Group. The stellar halo and globular cluster system of M31 are both well studied. Durrell et al. (2001) observed a large population of red giant branch stars in the halo of M31. Their resulting metallicity distribution function was bi-modal, dominated by a moderately high metallicity population ($[m/\mathrm{H}] \sim -0.5$) with a significant metal-poor population also present. Surprisingly, a comparison of the stellar halo metallicity distribution function with that of the globular cluster system reveals they do not match; the globular cluster system of M31 has a much larger fraction of metal-poor objects. A similar result is found for the halo of the giant elliptical galaxy NGC 5128 (Harris & Harris 2000). At a distance of 4 Mpc (Harris & Harris 2000), individual stars in the halo of NGC 5128 can be easily resolved with the Hubble Space Telescope.

The Local Group galaxy M33 in Triangulum has been studied relatively little in comparison to other members of the Local Group. M33 is small in comparison to M31 and the Milky Way; however, it is typical of spiral galaxies found throughout the universe. At a distance of 916 ± 17 kpc (Kim et al. 2002), it is relatively straight forward to perform photometry on the red giant branch stars in the halo of M33. Although significant for its size, the globular cluster system of M33 is rather sparse in comparison to the larger members of the Local Group, M31 and the Milky Way. Early studies of M33's globular cluster system by Christian & Schommer (1982, 1988) revealed a broad spectrum of cluster ages. More recently, Sarajedini et al. (2000) derived metallicities for 9 globular clusters in the halo of M33. The mean metallicity of their sample is $\langle[\mathrm{Fe/H}]\rangle = -1.27 \pm 0.11$ dex; however, there is a significant spread of metallicity in this sample. While the globular cluster system of M33 has been fairly well studied, very little work has been done on the stellar population in the halo. The work of Mould & Kristian (1986) represents one of the only studies of this population. Their analysis of a field 7 kpc from the galaxy center along the southeast minor

axis revealed a very metal poor population, with a mean metallicity of $[m/\mathrm{H}] = -2.2 \pm 0.8$ ([Fe/H] $\sim$ -1.9 dex using $[m/\mathrm{H}] \sim$ [Fe/H] + 0.3 from Durrell et al. (2001)). This mean does not compare well with the mean metallicity of the globular clusters (Sarajedini et al. 2000). Unfortunately, photometric incompleteness in their V-band data limited their ability to investigate the presence of metal rich stars.

Kinematic studies of the HI extent of M33 have revealed a significant "integral-shaped" warp in its disk. The warp begins at a distance of 5 kpc from the center of M33 and grows very quickly; at a distance of 10 kpc from the center, gas is rotating about an axis inclined at an angle of 40° relative to the inner disk (Rogstad et al. 1976). Given that the central disk of M33 has an inclination of $i = 55°$ (Deul & van der Hulst 1987), the outer disk is then nearly edge-on (outer disk inclination of $\sim 95°$). Of particular interest for this work is the presence of a sharp cut-off of the main HI disc along the eastern edge of the galaxy (Reakes & Newton 1978), since this will also result in a cutoff in the disk stars.

In this paper, we present new photometry of the stellar halo of M33. Utilizing the current generation of telescopes, our sample probes much deeper than previous stellar halo studies of M33, allowing a more complete investigation of the chemical composition of the halo. In Section 2 we discuss the observational details, subsequent data reduction, and classification of our data. In Section 3 we derive a luminosity function for the halo stars and use this to derive the distance to M33. In Section 4 the chemical composition of the halo is investigated through the derivation of the metallicity distribution function. The metallicity results are compared to those of the halo globular clusters and simple chemical evolution models are employed in an attempt to explain a possible formation scenario for M33.

2. Observations

V and I band CCD images of a single field in the halo of M33 were obtained on September 10, 1999 using the CFHT12K camera on the Canada-France-Hawaii Telescope (CFHT). The CFH12K is a wide-field mosaic CCD camera, which consists of 12 individual CCD chips, each 2k×4k pixels, arranged in a 2 chip× 6 chip pattern. The pixel size of 15 μm results in an image scale at the prime focus of 0.206 $''$pixel^{-1}, which yields a field of view of 7×14 arcmin^2 for an individual chip or 30×42 arcmin^2 for the entire camera. A total of 6 exposures of M33's halo were obtained in each filter, with individual exposure times of 900 seconds. Figure 1 shows the position on the sky of the mosaic image relative to the disk of

M33[1].

2.1. Data Preprocessing

Data preprocessing and calibration were performed with tasks in IRAF[2]. Preprocessing of the program images (bias and dark subtraction, flat fields, and geometric correction) involved operations on the entire mosaic with the mosaic reduction package *mscred*. Additional calibration images (twilight images, darks and bias frames) were obtained from the CADC archive[3]. Twilight sky images were used to create flat field frames and resulted in the program images being flattened to the ∼1%-2% level.

The *I*-band images contain significant fringing at the 3%-4% level due to interference within the CCD of atmospheric OH^- emission lines. Master fringe frames were created for each chip in the mosaic from the dithered M33 images. The master fringe frame was then subtracted from each individual chip and exposure. The individual chips of each exposure were then registered spatially and combined, with the exposure in each filter with the highest quality seeing being used as the reference image.

Large-format cameras, such as the CFH12k, also suffer from significant geometric distortion across their wide field of view. Rather than rescale the pixels, the distortion was removed through the use of correction images made available by the CFHT staff. Dividing the program images by the correction images rescales the sky level to produce consistent photometry across the entire mosaic.

2.2. Calibration

Photometric calibration was performed with stars in the open cluster NGC 7790 (Stetson Photometric Standard Fields[4]). The majority of the NGC 7790 field was imaged on a single

[1]M33 image obtained from the Digital Sky Survey, made available by the Space Telescope Science Institute.

[2]Image Reduction and Analysis Facility. IRAF is distributed by the National Optical Astronomy Observatories, which are operated by the Association of Universities for Research in Astronomy, Inc., under cooperative agreement with the National Science Foundation. `http://iraf.noao.edu/`

[3]Guest User, Canadian Astronomy Data Center, which is operated by the Dominion Astrophysical Observatory for the National Resarch Council of Canada's Herzberg Institute of Astrophysics.

[4]The CADC Astronomical Standards Page: `http://cadcwww.dao.nrc.ca/standards/`

chip of the mosaic (chip 02). The standards were fit to the usual transformation equation:

$$M_n = m_n + a_n + b_n X + c_n(V - I) + \Delta V_{2,n} \quad (1)$$

where M_n is the calibrated magnitude, m_n is the aperture corrected instrumental magnitude (using an aperture radius of 15 pixels), a_n is the zero-point correction, b_n is the extinction coefficient, c_n is the colour coefficient, X is the effective airmass of the exposures, and $(V-I)$ is the instrumental colour, all with respect to chip n. An average value of the extinction coefficient was adopted from Landolt (1992). The same color coefficient was used for each chip, based on the solution from chip 2, and a simple zero-point correction determined from the relative sky levels between chip 2 and the remaining chips was applied to the other chips in each filter, represented by $\Delta V_{2,n}$ in the transformation equation. The resulting values for the various coefficients are summarized in Table 1. The transformation equations also require the use of a single airmass value, which was determined from $X_{eff} = \frac{1}{6}(X_{init} + 4X_{mid} + X_{end})$ (Stetson 1989).

2.3. Photometry and Classification

All photometric reductions on the final M33 images were performed with stand-alone versions of the DAOPHOT II and ALLSTAR packages (Stetson 1987; Stetson, Davis & Crabtree 1990; Stetson 1992). A first pass with DAOPHOT II and ALLSTAR with a detection threshold of 6 σ above sky was performed, followed by a second pass, which did not add significantly to the number of detections. A stellar point spread function (PSF) was derived for each chip individually with 10 to 20 bright and isolated stars on each chip. The PSF did not vary significantly across a single chip and so a constant PSF was used for each chip. Aperture corrections were defined with 5 to 10 bright, isolated stars on each chip with an aperture radius of 15 pixels.

The reduction routines employed by DAOPHOT II discard any obviously nonstellar objects; however, many slightly resolved background galaxies can still be present. Removal of these objects was accomplished with the χ parameter from DAOPHOT II (Stetson 1987) and the r_1 and r_{-2} radial moments (Kron 1980; Harris et al. 1981). The χ parameter measures the PSF fitting quality, while the r_1 and r_{-2} radial moments examine the extended distribution and the central concentration of the light, respectively. Galaxies have a more extended distribution and are less centrally peaked than stars. The range of χ, r_1, and r_{-2} values that defined the stellar population were derived for each chip in each filter using the results of artificial star experiments (see Section 2.4). Only objects that met these criteria were retained for the remainder of the analysis. The resulting *I,(V-I)* color-magnitude diagram of the M33 halo field is shown in Figure 2.

2.4. Artificial Star Experiments

The integration of data from different chips in a CCD mosaic presents some unique issues in characterization of the data. For example, the quantum efficiencies of each chip differ, which results in varying photometric uncertainties and incompleteness levels. To properly quantify these effects, we have used the commonly employed method of adding artificial stars of known magnitudes to the science frames and re-reducing the images. In addition, to fully characterize the incompleteness, the artificial star experiments were performed for a range of I magnitude and $V - I$ color. A total of 56,000 stars were added to each chip in the mosaic over a series of 14 runs and over a two dimensional grid on the color-magnitude diagram covering the range $20.9 < I < 24.9$, $0.14 < (V - I) < 3.14$. The artificial star frames were then reduced with the same procedures used for the original science images. The color-magnitude diagram of recovered artificial stars for one of the chips is shown in Figure 3.

The 50% completeness level determined from the artificial star tests is defined as the limiting magnitude, m_{lim}, and was derived by fitting the data with the following interpolation function (Fleming et al. 1995)

$$f(m) = \frac{1}{2}\left[1 - \frac{\alpha(m - m_{\rm lim})}{\sqrt{(1 + \alpha^2(m - m_{\rm lim})}}\right] \tag{2}$$

where m represents the V or I magnitude and α is a shape parameter that determines how sharply $f(m)$ decreases (typically 3.0 to 4.0 for this data). The limiting magnitudes V_{lim} and I_{lim} for each of the chips are summarized in Table 2. The photometric incompleteness for each individual star in Figure 2 was obtained by linear interpolation from the incompleteness $f(I, V - I)$ found for the grid points as determined by the artificial star tests for each chip.

3. The Luminosity Function and the Distance to M33

The significant warp of M33's disk results in an abrupt radial cutoff in the disk population. This cutoff was confirmed by examining star counts as a function of radial distance from the center of M33. The star counts drop precipitously across chips 00 and 06 (the two closest to the nucleus of M33), which corresponds to the sharp terminus exhibited by the HI disk (Reakes & Newton 1978). Figure 4 demonstrates that the star counts in the remaining 10 chips show a clear dropoff as a function of radius in the M33 halo, assuring us that we are indeed observing primarily a halo population and not a foreground or background population.

To deal effectively with the problem of contamination due to faint, unresolved background galaxies and foreground stars, we used a background field from the study of M31 by Durrell et al. (2001). In examining the stellar halo of M31, Durrell et al. (2001) imaged a background field (labeled $\mathscr{R}1$ in their paper) sufficiently distant from M31 to be free of M31 stars. The $\mathscr{R}1$ and M33 fields lie at significantly different Galactic latitudes ($b = -21^\circ$ and $b = -31^\circ$ respectively) and so the Galactic foreground contamination differs between the two fields. The color magnitude diagram for the $\mathscr{R}1$ field is shown in Figure 5; this color-magnitude diagram has also been cleaned of nonstellar objects.

The foreground reddening, $E(V-I)$, of the M33 field is also expected to differ from that of the adopted background field. From the local HI column densities from Burstein & Heiles (1984), the reddening of M33 is $E(B-V) = 0.04$. Adopting the relations $E(V-I) = 1.35E(B-V)$ and $A_I = 1.95E(B-V)$ (Cardelli et al. 1989; Barmby et al. 2000) yields a reddening of $E(V-I) = 0.054$ and extinction $A_I = 0.078$ for M33. The reddening for the $\mathscr{R}1$ field from the same source is $E(V-I) = 0.08$, which results in a differential reddening of $E(V-I) = 0.026$ between the two fields.

The onset of core helium flash in low mass stars marks the bright tip of the red giant branch. This sharp transition is evident as a sudden upturn in the luminosity function of an old stellar population and so can be used to determine accurate distances (Frogel et al. 1983). Before applying this method to the M33 halo field, it is useful to subtract the $\mathscr{R}1$ luminosity function from that of the M33 halo. To account for the differential reddening, $\Delta I = 0.042$ and $E(V-I) = 0.026$ were subtracted from the $\mathscr{R}1$ data. The completeness-corrected luminosity function was then constructed by applying the interpolated completeness factor, $f(I, V-I)$, to give each star an effective count of $1/f$. Subtraction of the $\mathscr{R}1$ field was dealt with by an iterative process to account for the difference in Galactic foreground contamination (simply scaling the two fields by their relative area overcorrects for foreground contamination). Ideally, the luminosity function should average to zero at the bright end, since this part of the luminosity function is dominated by foreground Milky Way stars in both fields. We thus varied the scaling factor over a range of 0.8 to 1.4 until the average number counts were zero at the bright end of the luminosity function after background subtraction. Stars over the magnitude range $19.0 \leq I \leq 20.5$ were used to derive this scale factor, which was then applied to the $\mathscr{R}1$ luminosity function before subtraction from the M33 halo luminosity function. The final completeness corrected luminosity function for the M33 halo is shown in Figure 6.

The magnitude of the tip of the red giant branch was found with an edge-detection algorithm, which uses a numerical second derivative to locate the abrupt change in slope associated with a sudden increase in the number of stars at this magnitude. To test the

sensitivity of this method to the details of the background subtraction scaling, we used a range of scale factors to perform the background subtraction and then applied the edge detection algorithm to each case.

In all cases, the tip of the red giant branch was found repeatably at the same I magnitude, $I_{TRGB} = 20.7 \pm 0.1$ mag. Adopting an absolute magnitude turnoff of $M_{I,TRGB} = -4.1 \pm 0.1$ mag based on Milky Way globular cluster data (Harris et al. 1998, 1999) and using the derived extinction ($A_I = 0.078 \pm 0.029$ mag) yields a distance modulus for M33 of $(m - M)_0 = 24.72 \pm 0.14$ mag. This distance modulus is in good agreement with the recent HST I-band observations of Cepheids in M33 by Lee et al. (2002), which gives a distance modulus of $(m - M)_0 = 24.52 \pm 0.14(random) \pm 0.13(systematic)$. Other recent results based on HST photometry of M33 disk stars in the V and I-bands give a distance modulus of $(m - M)_0 = 24.81 \pm 0.04(random)^{+0.15}_{-0.11}(systematic)$ (Kim et al. 2002) using the tip of the red giant branch.

4. The Metallicity of the Halo of M33

4.1. The Stellar Metallicity Distribution Function

Deriving the metallicity distribution function requires us to assume that the M33 halo stars are old. The observed distribution of stars in the color-magnitude diagram is a result of several factors, including photometric scatter, a possible range of stellar ages, and a range of stellar composition. The fiducial grid of red giant branch tracks used in this work applies to old stars ($\tau > 10$ Gyr); with this assumption, only the metallicity of a model star determines its location in the color-magnitude diagram. Evolutionary tracks from VandenBerg et al. (2000) were used within an interpolation code (Harris & Harris 2000) to determine stellar metallicities.

The color-magnitude diagrams of the M33 halo and the $\mathscr{R}1$ fields are shown overlaid with the evolutionary tracks for 0.8 $M_\odot$ stars from VandenBerg et al. (2000), which range from [Fe/H] = −2.31 to −0.04. A single metal-rich isochrone ([Fe/H] = +0.07) was added to the model grid from Bertelli et al. (1994) to allow the identification of any metal-rich halo stars. Following the method of Durrell et al. (2001) and Harris & Harris (2000), the $(V - I)$ color of each model was empirically shifted by -0.03 to match the observed red giant branch distributions of Milky Way globular clusters over the full metallicity range.

For the metallicity interpolation, the model grid was first shifted by the distance modulus of M33 [$(m-M)_I = 24.8$] and the foreground reddening ($E(V-I) = 0.054$). The metallicity of each individual star was determined by bi-linear interpolation between evolutionary tracks

in the model grid. Each star was first transformed from the $(M_I, (V-I))_\circ$ plane to the $(M_{bol}, (V-I)_\circ)$ plane through the relation:

$$M_{bol} = M_I + (V-I)_0 - BC_I$$

where BC_I is the bolometric correction for the star in the I-band (Harris & Harris 2000). The bolometric corrections are provided with the stellar models and these points are interpolated to generate the bolometric correction for the star. The two evolutionary tracks bracketing the star were identified and interpolation between these tracks was performed within the $(M_{bol}, (V-I)_\circ)$ plane.

Metallicities were obtained for all of the stars in the color-magnitude diagram over a magnitude range of $20.5 < I < 22.5$ mag. Stars more than 0.02 mag bluer than the most metal-poor track, as well as stars near the RGB tip (where interpolation is more uncertain) were not used in the analysis. At fainter I magnitudes ($I > 22.5$), photometric uncertainties and field contamination increase, and so the fainter end of the color-magnitude diagram was not used for the metallicity distribution function analysis. At the bright end above the red giant branch tip, the color-magnitude diagram is dominated by contamination due to field stars that have survived the background subtraction procedure. Additionally, few M33 halo stars are expected to be seen above the tip of the red giant branch; the bright cutoff used in the derivation of the metallicity distribution function reflects this.

After metallicities were determined, the resulting star counts were corrected for photometric incompleteness, background subtracted, and then binned in 0.1 dex metallicity bins to give the distribution shown in Figure 7. A single component Gaussian was fit to this metallicity distribution function, which identified a distinct, metal-poor peak at $[m/\mathrm{H}] = -0.94$ with a reduced chi squared of $\chi^2 = 1.4$. The M33 halo population shows no indication of multi-modality in its metallicity distribution function. A comparison of the raw and background subtracted metallicity distribution functions reveals that the peak at $[m/\mathrm{H}] \approx -0.9$ is seen even without background correction and thus is almost certainly due to the halo of M33.

At the metal-rich end (at $[m/\mathrm{H}] \geq -0.4$), the counts become more uncertain and the background field may not adequately remove the contamination from background galaxies. It is unlikely that we are seeing a mix of halo and disk stars, because, as described in Section 1, M33 has a significant disk warp which has the effect of creating a rather sharp cutoff between the disk and halo. Contamination may be present in the chips closest to M33; however, this contamination is limited to chips 00 and 06, since the long axis of the mosaic is oriented along the minor axis of M33. The combination of these factors could well be responsible for the excess counts seen in the most metal-rich bins. However, the remaining analysis will not

be significantly impacted by the uncertainties in these few metal-rich bins.

At the metal-poor end ($[m/\mathrm{H}] \leq -1.7$), there is expected to be a population of asymptotic giant branch (AGB) stars which would make the residual counts higher there. A close look at the lifetimes of the stars along these two tracks over the range of metallicities used here shows that, of the total sample, approximately $20\% \pm 3\%$ stars will be asymptotic giant branch stars [a similar result to that of Harris et al. (1999)]. Comparison of the AGB tracks and red giant branch (RGB) tracks of Girardi et al. (2000) over a range of metallicities and masses reveals the AGB tracks to average ≈ 0.1 mag bluer in $(V-I)$ color than the RGB tracks. If we consider the AGB stars have the same intrinsic metallicity peak as the RGB population, then the metallicities of the aymptotic giant branch stars would be interpolated to be ≈ 0.15 dex more metal poor than the RGB stars. This effect would tend to broaden and bias the metallicity distribution function, but only slightly.

4.2. Comparison with the Globular Cluster System

In comparison with the larger spirals of the Local Group, M33 has a rather sparse globular cluster system, which has, however, been studied much more extensively than the halo stars in M33. Christian & Schommer (1982, 1988) performed photometry on 130 candidate clusters and identified 27 as possible old clusters (> 10 Gyr). Unlike the globular cluster systems of M31 and the Milky Way, Christian & Schommer found M33 to have relatively massive clusters of all ages. They concluded that cluster formation for globular clusters younger than 10 Gyr was fairly continuous. Later work by Schommer et al. (1991) showed the ages of the globular clusters traced their kinematics, with old globular clusters found in halo-like orbits and younger clusters in disk-like orbits.

More recent studies of the globular cluster system of M33 using HST by Sarajedini et al. (2000) have measured metallicities for nine globular clusters with ages ≥ 4 Gyr (Christian & Schommer 1988) in the halo of M33. The current sample of M33 globular clusters with measured metallicities is small and so we can only compare the bulk properties of the cluster and halo star populations. The mean metallicity of this sample of globular clusters is $\langle[\mathrm{Fe/H}]\rangle = -1.27 \pm 0.11$ dex, which is close to the mean determined for the halo stars in this work, $\langle[\mathrm{Fe/H}]\rangle = -1.24 \pm 0.04$ dex (using $[m/\mathrm{H}] \sim [\mathrm{Fe/H}] + 0.3$ from Durrell et al. (2001)). There is also a significant spread of metallicity in the halo globular clusters, similar to that seen in the halo stars.

4.3. Results from Chemical Evolution Models

We now compare the metallicity distribution function for the halo of M33 with a simple chemical evolution model. In a "closed-box" chemical evolution model (Searle & Sargent 1972; Pagel & Patchett 1975), the cumulative distribution of stellar abundance, Z, is given by

$$N(Z) \sim const\ \frac{1 - e^{-(Z-Z_\circ)/y}}{1 - e^{-(Z_N-Z_\circ)/y}} \tag{3}$$

where N is the number of stars with a metal abundance less than Z, $Z_\circ$ is the initial metal abundance of the gas, Z_N is the current metal abundance of the gas, and y is the yield ratio [the mass of gas in metals expelled by massive stars divided by the mass of dead stellar remnants (Pagel & Patchett 1975)]. "Leaky-box" models use an effective yield, y_{eff}, given in terms of the yield ratio and a parameter c that describes the fraction of mass lost from the box, that is, $y_{eff} = y/(1 + c)$. The mass loss is thought to be driven by supernovae and winds from massive stars, which shock the resident gas, expelling it from the idealized closed box model (Hartwick 1976). The functional form of the differential abundance distribution remains the same with y replaced by y_{eff} in equation 3. When fitting the leaky-box model to the M33 data, we use the differential distribution dN/dZ

$$\frac{dN}{dZ} \sim const\ \frac{e^{-(Z-Z_\circ)/y_{eff}}}{y_{eff}(1 - e^{-(Z_N-Z_\circ)/y_{eff}})} \tag{4}$$

Since the expression is in terms of Z, it is more natural to express the metallicity distribution function as a linear function of $(Z/Z_\odot)$, as shown in Figure 8. We kept the initial and current metal abundance fixed during the model fitting ($Z_\circ = 0$ and $Z_N = 0.0172$, respectively). The best-fit value of the effective yield, y_{eff}, was found to be $y_{eff} = 0.0024 \pm 0.0002$ and the resulting fit is represented by the solid line in Figure 8. Bin-to-bin deviations exist, but given the size of the error bars, these are not significant. The leaky-box model proves to give an excellent fit to the data.

A similar analysis using a "leaky box" model has been performed for M31 (Durrell et al. 2001) and the Milky Way (Ryan & Norris 1991). The value of the effective yield for the M33 halo clearly lies between the values for M31 and the Milky Way. Ryan & Norris (1991) find best fit values of y_{eff} to be ~ 0.0009 for the Milky Way's halo, while Durrell et al. (2001) find a best fit value of $y_{eff} = 0.005$ for M31. If the Milky Way and M31 had similar intrinsic yields, their c values would then differ considerably, which would imply that the Milky Way expelled a much larger fraction of the initial gas in its halo during its assembly. By the same token, M33 was not as efficient as the Milky Way in expelling its gas, but was about twice as efficient as M31. Thus, the enrichment of the halo of M33 was able to proceed to a greater

degree than in the Milky Way. Given the relatively shallow gravitational potential well of M33, it is surprising that M33 was better at retaining its gas than was the Milky Way.

Early studies of the halo of our Galaxy by Eggen et al. (1962) argued for a single, radial collapse of a proto-Galactic gas cloud. This process would leave a distinct metallicity gradient, since the formation of stars during the collapse would proceed from increasingly metal-rich gas. Schommer (1993) found some evidence for a radial metallicity gradient among old globular clusters. However, Sarajedini et al. (2000) found no support for this conclusion; in both cases, the sample sizes are quite small. If M33 does, in fact, lack a metallicity gradient, this would support the idea that M33 was formed by a build-up of smaller, spheroidal systems rather than a single, radial collapse. Unfortunately, the size of our stellar sample does not permit a statistically reliable constraint on the presence or absence of a metallicity gradient in the halo of M33.

5. Summary

We have presented the results of $(I, V-I)$ photometry of the halo stars of M33 in a field located 10 kpc from the galaxy center along its southeast minor axis. The stellar halo population was isolated through the use of image classification and a background field provided by Durrell et al. (2001). With an assumed reddening of $E(V-I) = 0.054 \pm 0.020$, the distance modulus based on the tip of the red giant branch was found to be $(m-M)_\circ = 24.72 \pm 0.14$ mag.

Through the use of a grid of red giant branch stellar models, metallicity values for individual stars were interpolated allowing the derivation of the halo metallicity distribution function. The metallicity distribution function shows a distinct peak at $[m/\mathrm{H}] = -0.94 \pm 0.042$ (or $\langle[\mathrm{Fe/H}]\rangle = -1.24 \pm 0.04$ dex (using $[m/\mathrm{H}] \sim [\mathrm{Fe/H}] + 0.3$ from Durrell et al. (2001)) and agrees well with the mean metallicity measured for nine M33 globular clusters of $\langle[\mathrm{Fe/H}]\rangle = -1.27 \pm 0.11$ by Sarajedini et al. (2000).

A single component leaky box chemical evolution model provides a good fit to the metallicity distribution, resulting in a yield of $y_{eff} = 0.0024$. Comparison of the yield of M33 with those of M31 and the Milky Way ($y_{eff} = 0.0009$ and 0.005, respectively) places the M33 yield between these values. It is somewhat surprising that M33 has a higher effective yield compared to the Milky Way, since it has a significantly smaller potential well to confine its gas. However, if the halos of these galaxies were built up from the accretion of smaller satellites, an alternate interpretation would be that the subsystems were smallest for the Milky Way, larger for M33, and still larger for M31 (from the standard mass-metallicity

relation for dwarf galaxies).

We would like to thank Pat Durrell for making available the M31 background data and for several fruitful discussions concerning the reduction of CFHT12K data. This research was supported by NSERC research grants to C. D. W. and W. E. H., and R. S. B. gratefully acknowledges financial support from C. D. W. We also acknowledge the use of archival data made available by the Canadian Astronomy Data Centre, which is operated by the Herzberg Institute of Astrophysics, National Research Council of Canada.

REFERENCES

Barmby, P., Huchra, J. P., Brodie, J. P., Forbes, D. A., Schroder, L. L., & Grillmair, C. J., 2000, AJ, 119, 727

Bertelli, G., Bressan, A., Chiosi, C., Fagotto, F., and Nasi, E., 1994, A&AS, 106, 275

Burstein, D., & Heiles, C., 1984, ApJS, 54 33

Cardelli, J. A., Clayton, G. C., & Mathis, J. S., 1989, ApJ, 345, 245

Christian, C. A., Schommer, R. A., 1982, ApJS, 49 405

Christian, C. A., Schommer, R. A., 1988, AJ, 95, 704

Deul, E. R., van der Hulst, J. M., 1987, A&AS, 67, 509

Durrell, P. R., Harris, W. E., and Pritchet, C. J., 2001, AJ, 121, 2557

Eggen, O., Lynden-Bell, D., & Sandage, A. R., 1962, AJ, 136, 748

Fleming, D. E. B., Harris, W. E., Pritchet, C. J., & Hanes, D. A., 1995, AJ, 109, 1044

Frogel, J. A., Cohen, J. G., Persson, & S. E., 1983, ApJ, 275, 773

Girardi, L., Bressan, A., Bertelli, G., & Chiosi, C., 2000, A&AS, 141, 371

Harris, W. E., Fitzgerald, M. P., & Reed, B. C. 1981, PASP, 93, 507

Harris, G. L. H., Harris, W. E., 2000, AJ, 120, 2423

Harris, G. L. H., Harris, W. E., and Poole, G. B., 1999, AJ, 117, 855

Harris, W. E., Durrell, P. R., Pierce, M. J., and Secker, J., 1998, Nature, 395, 45

Harris, W. E., 2001, in Star Clusters, Saas-Fee Advanced Course 28 (New York: Springer), ed. L.Labhardt & B.Binggeli

Hartwick, F. D. A., 1976, ApJ, 209, 418

Kim, M., Kim, E., Lee, M. G., Sarajedini, A., and Geisler, D., 2002, AJ, 123, 244

Kron, R. G., 1980, ApJS, 43, 205

Landolt, A. U., 1992, AJ, 104, 340

Lee, M. G., Kim, M., Sarajedini, A., Geisler, D., & Gieren, W., 2002, ApJ, 565, 959

Mould, J., & Kristian, J., 1986, ApJ, 305, 591

Pagel, B. E. J., & Patchett, B. E., 1975, MNRAS, 172, 13

Reakes, M. L., Newton, K., 1978, MNRAS, 185, 277

Rogstad, D. H., Wright, M. C. H., and Lockhart, I. A., 1976, ApJ, 204, 703

Ryan, S. G., & Norris, J. E., 1991, AJ, 101, 1865

Sarajedini, A., Geisler, D., Schommer, R., Harding, P., 2000, AJ, 120, 2437

Schommer, R. A., 1993, ASP Conf. Ser. 48, The Golbular Cluster-Galaxy Connection, ed. G. H. Smith & J. P. Brodie (San Francisco: ASP), 458

Schommer, R. A., Christian, C. A., Caldwell, N., Bothun, G. D., & Huchra, J., 1991, AJ, 101, 873

Searle, L., & Sargent, W. L., 1972, ApJ, 173, 25

Stetson, P. B., 1987, PASP, 99, 191

Stetson, P. B., 1992, in ASP Conf. Ser. 25, Astronomical Data Analysis Software and Systems I, ed. D. M. Worral, C. Biemesderfer, & J. Barnes (San Francisco: ASP), 297

Stetson, P. B., Davis, L. E. & Crabtree, D. B., 1990, in CCDs in Astronomy, ASP Conf. Ser. 8, Jacoby G.H., (ASP, San Francisco), p.289

Stetson, P. B., 1989, in Some Factors Affecting the Accuracy of Stellar Photometry with CCDs (And Some Ways of Dealing with them), in Highlights of Astronomy, 8, 635, ed. D. McNally

VandenBerg, D. A., Swenson, F. J., Rogers, F. J., Iglesias, C. A., and Alexander, D. R., 2000, ApJ, 532, 430

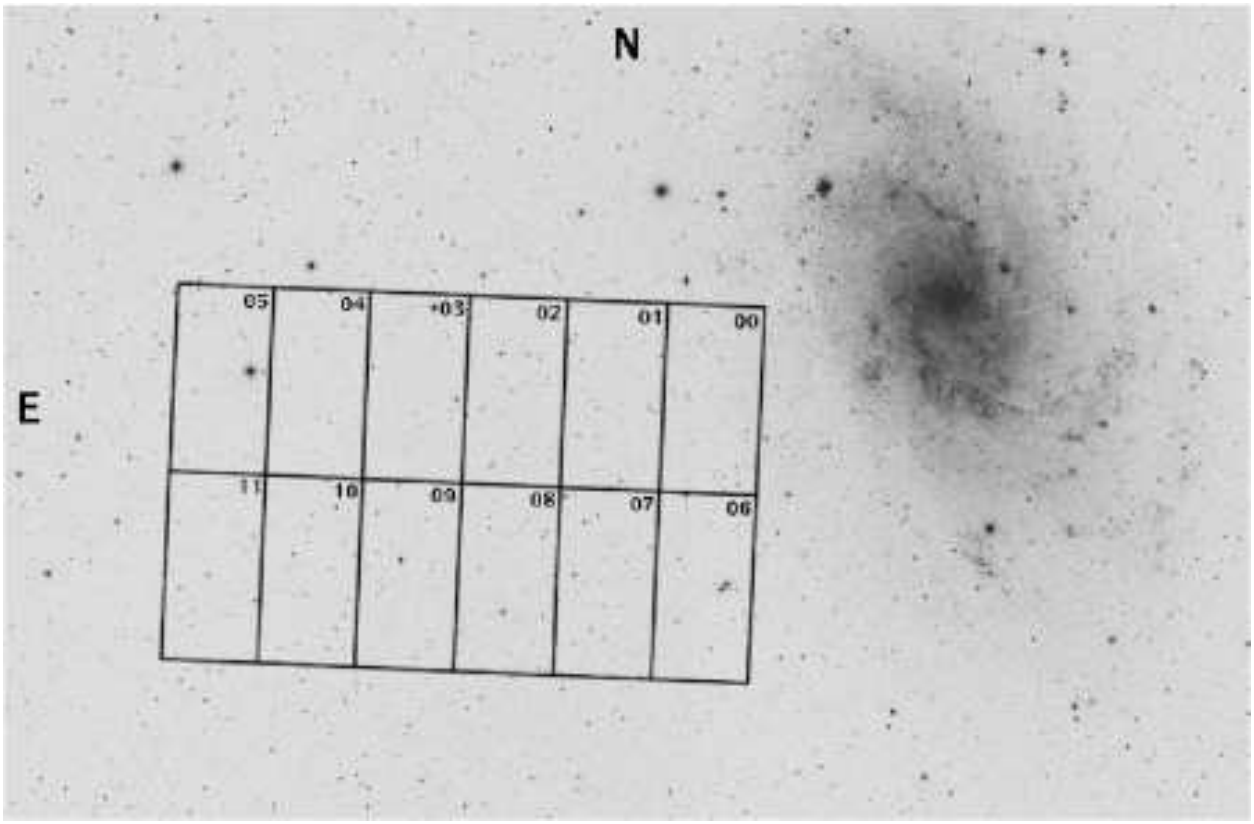

Fig. 1.— Location of the CFH12k mosaic relative to the disk of M33.

Table 1. Transformation Coefficients

	a_n	b_n	c_n
V	1.319 ± 0.003	0.016 ± 0.003	-0.152
I	1.012 ± 0.005	-0.016 ± 0.005	-0.061

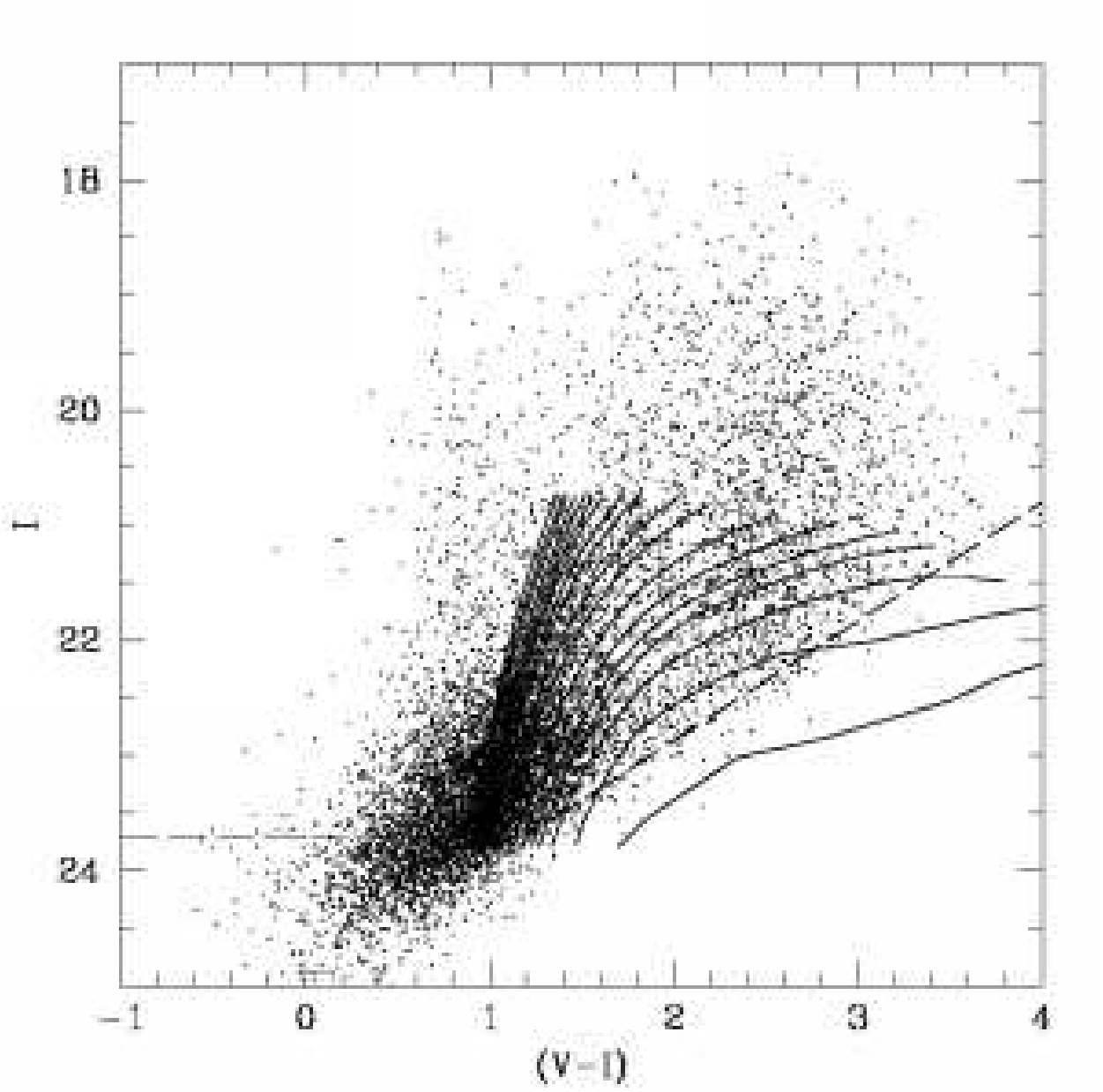

Fig. 2.— $I, (V - I)$ color magnitude diagram of the M33 halo field after rejection of all nonstellar objects. The dashed line marks the average 50% completeness level and solid lines show the theoretical models from VandenBerg et al. (2000). The two CCD chips closest to the center of M33 suffer from substantial contamination by disk stars and are not included here.

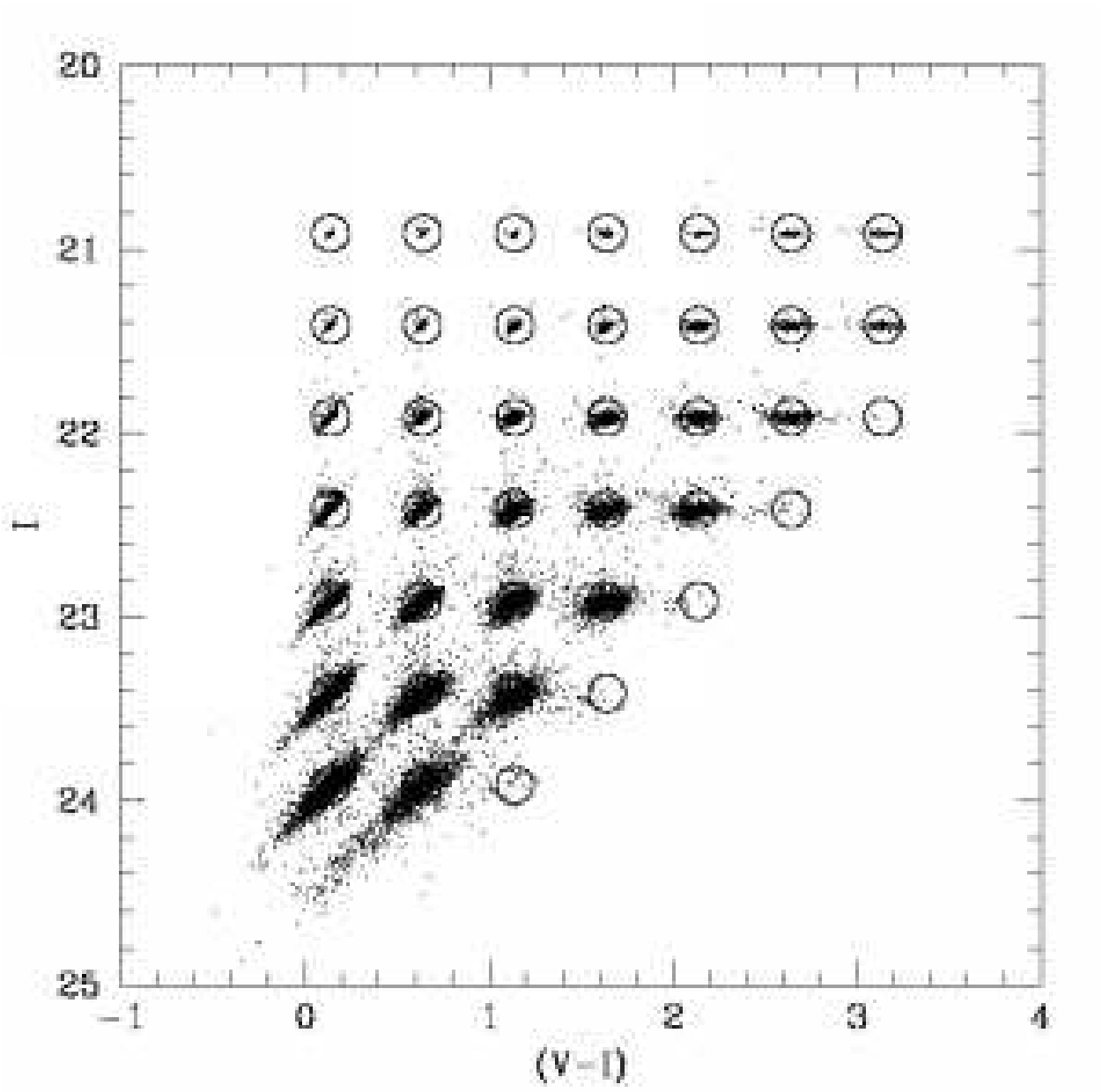

Fig. 3.— An example of the color-magnitude diagram of stars recovered from the artificial star tests. The circles are centered on the locations of the added stars and the points represent the recovered stars.

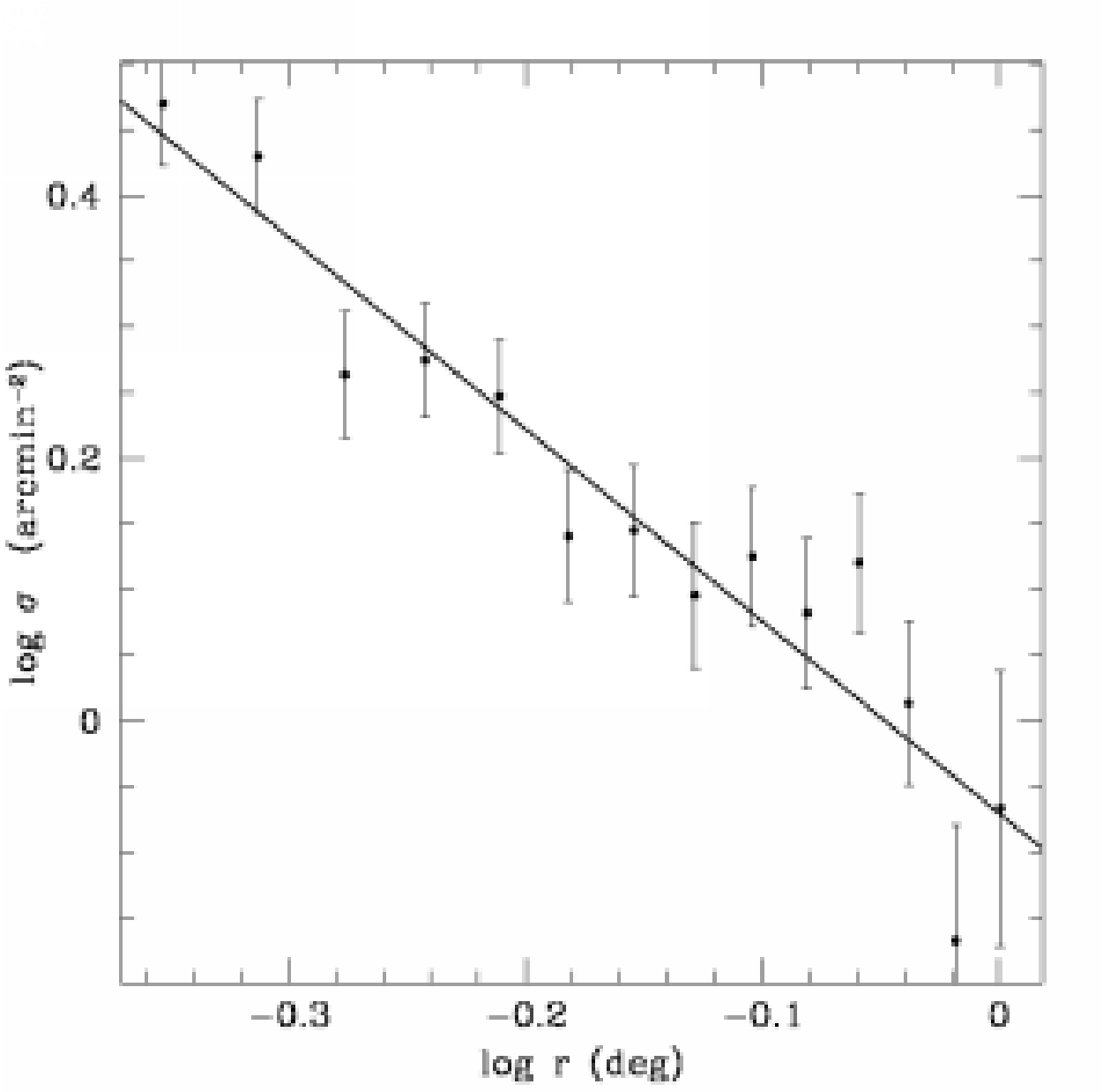

Fig. 4.— Log-log plot of the stellar number density in the metallicity distribution function with magnitudes in the range $20.5 < I < 22.5$ as a function of radius from the galactic center of M33. The solid line is the least-squares best fit to the profile, with a slope of -1.46 ± 0.14.

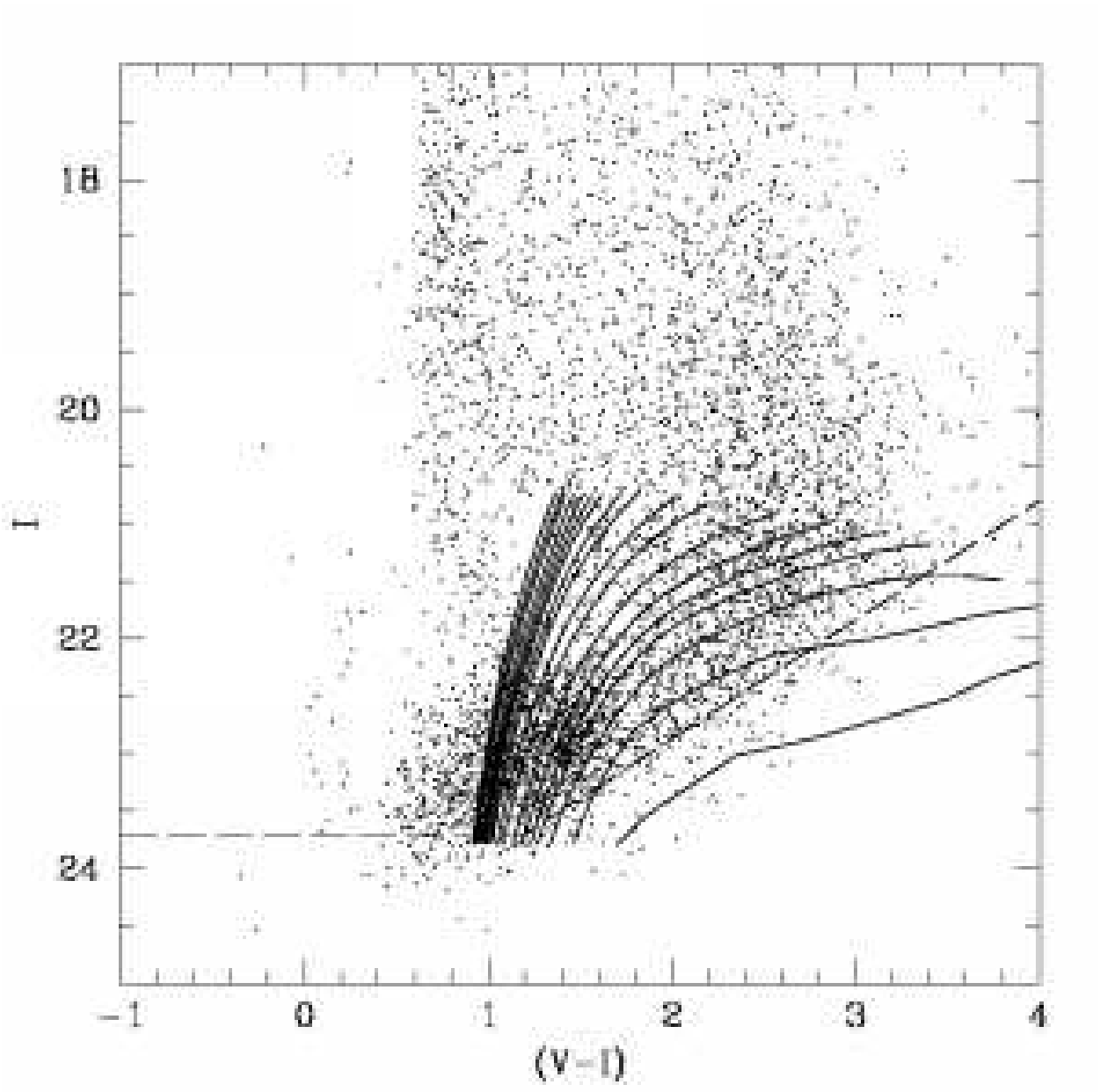

Fig. 5.— Color magnitude diagram of adopted background field near M31, from Durrell et al. (2001). The dashed line marks the 50% completeness level and the solid lines show the theoretical models from VandenBerg et al. (2000).

Table 2. Limiting Magnitudes

CCD No.	V_{lim}	I_{lim}	CCD No.	V_{lim}	I_{lim}
01	24.67	23.59	07	24.72	23.92
02	24.76	24.06	08	24.71	23.92
03	25.03	24.25	09	24.85	23.96
04	24.62	23.95	10	24.72	23.85
05	24.84	24.01	11	24.73	23.95

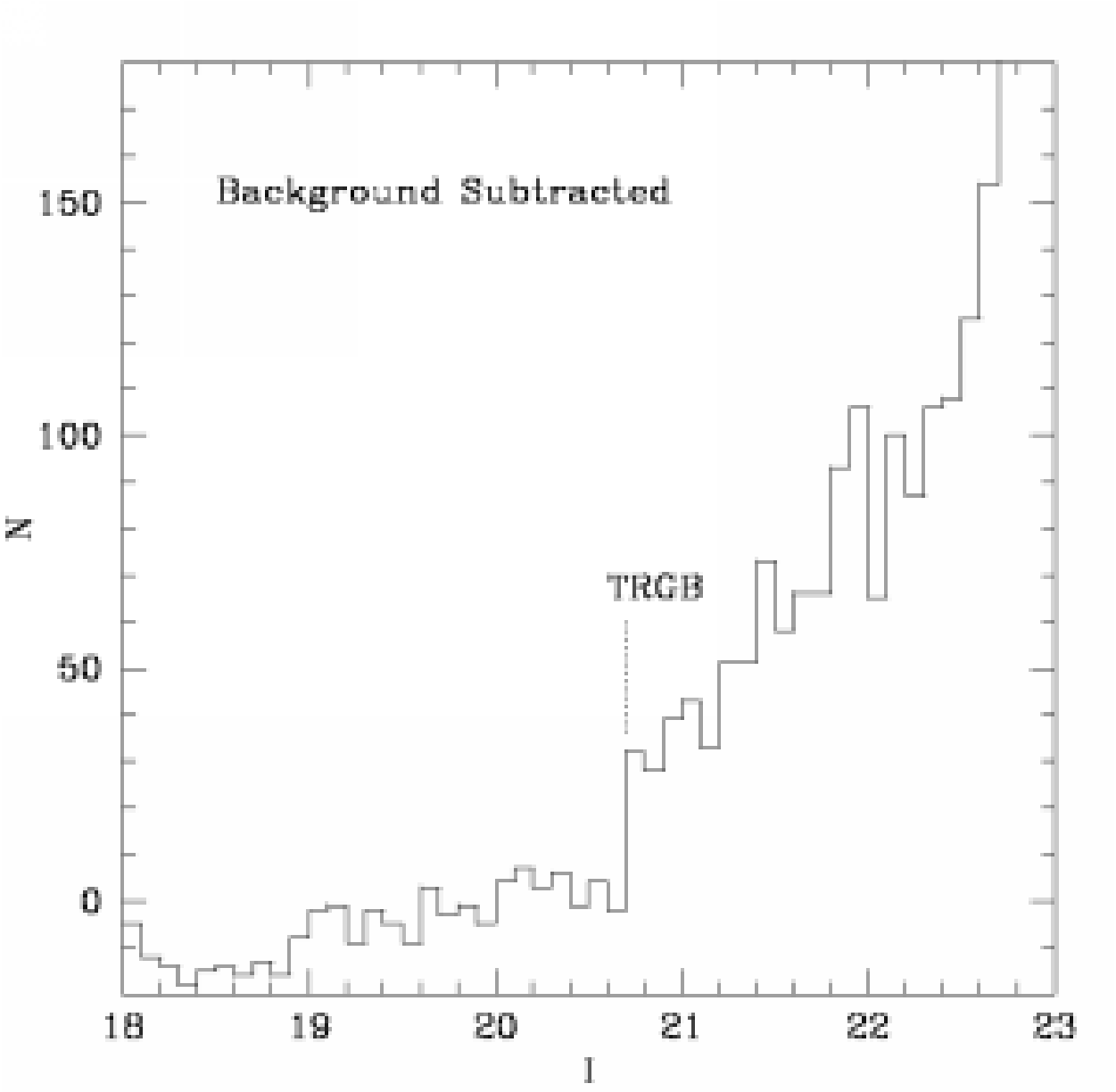

Fig. 6.— The completeness corrected I-band luminosity function in the halo of M33. The location of the tip of the red giant branch is indicated; in the M33 halo it is seen at $I_{TRGB} = 20.7$. Contamination by background galaxies has been removed as described in Section 3.

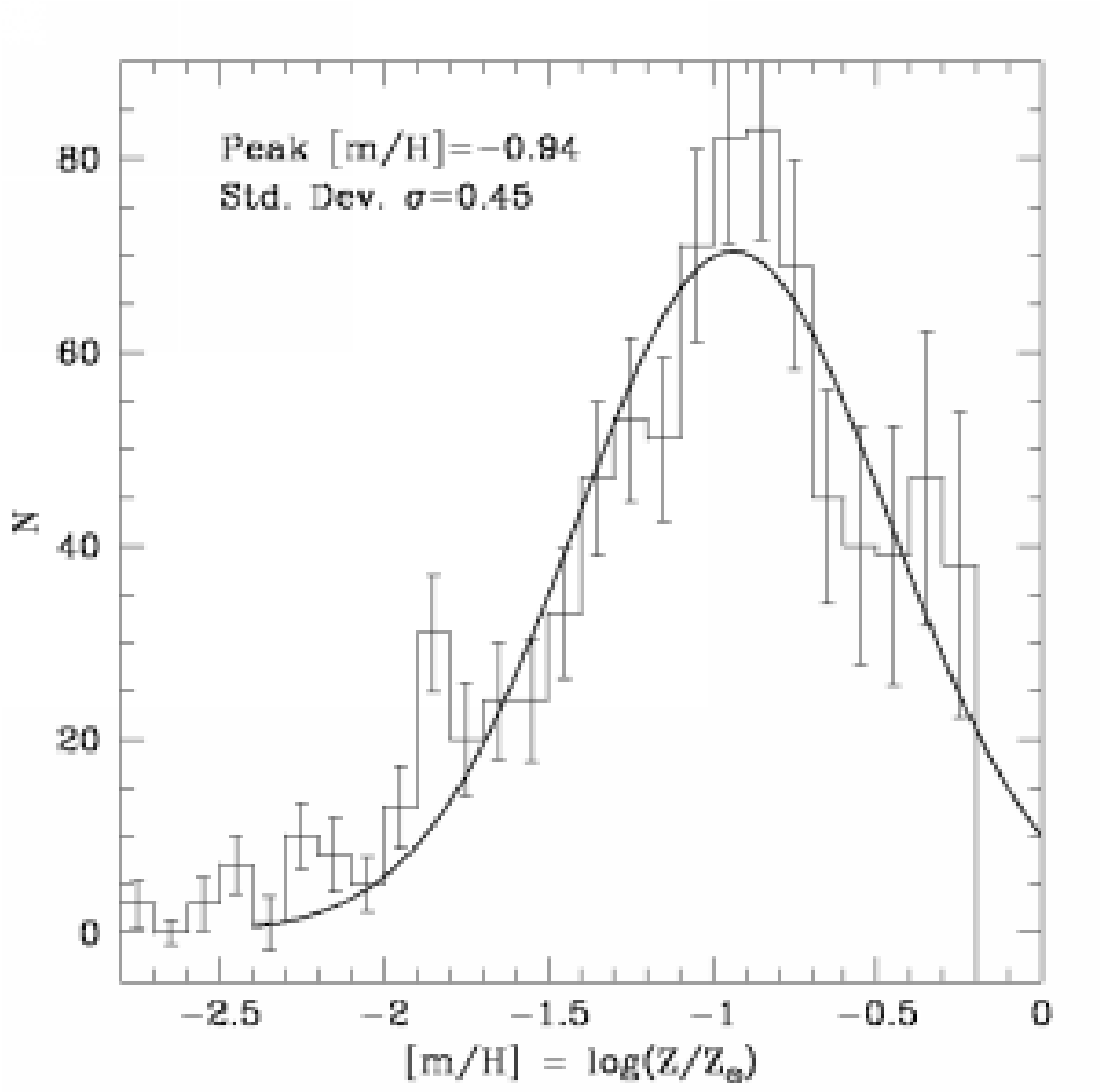

Fig. 7.— The completeness corrected metallicity distribution function of the halo of M33. The best fit Gaussian is shown with a mean of [m/H] = −0.94. These counts have been corrected for background contamination. The error bars correspond to Poisson statistics.

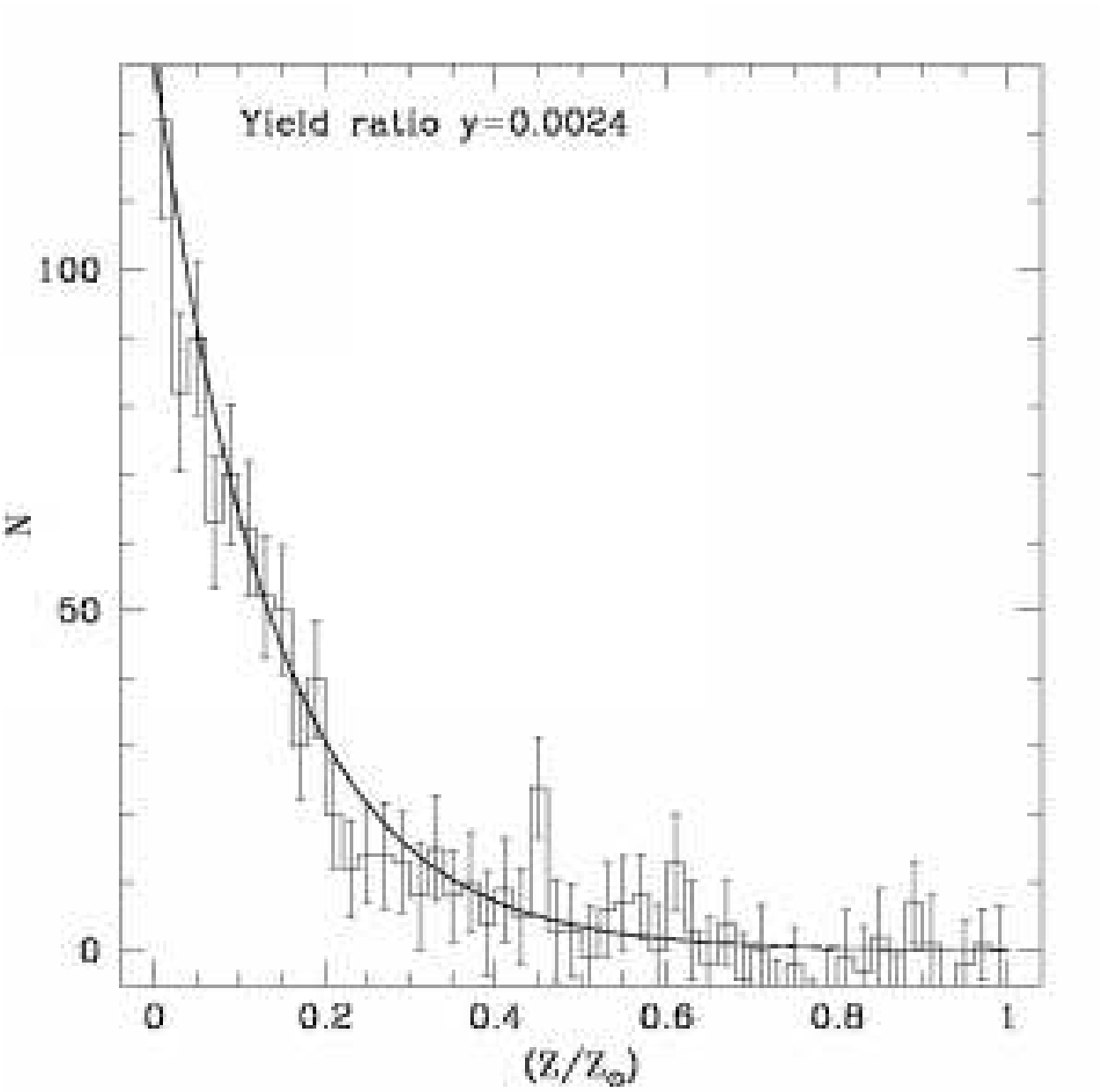

Fig. 8.— Metallicity distribution function of M33 halo stars on a linear $(Z/Z_{\odot})$ scale. The best-fit closed box model is the solid line, with a yield ratio of $y = 0.0024$. The reduced chi squared of the fit is $\chi^2 = 1.1$.